Journal of Power Sources 196 (2011) 10484–10489

Contents lists available at SciVerse ScienceDirect

Journal of Power Sources

journal homepage: www.elsevier.com/locate/jpowsour

Aqueous dispersed conducting polyaniline nanofibers: Promising high specific capacity electrode materials for supercapacitor

Hongming Zhang, Qiang Zhao, Shuiping Zhou, Nianjiang Liu, Xianhong Wang*, Ji Li, Fosong Wang

Key Laboratory of Polymer Ecomaterials, Changchun Institute of Applied Chemistry, Chinese Academy of Sciences, Changchun 130022, PR China

ARTICLE INFO

Article history:
Received 25 April 2011
Received in revised form 26 July 2011
Accepted 16 August 2011
Available online 22 August 2011

Keywords:
Polyaniline nanofibers
Electrode material
Supercapacitor
Aqueous dispersion

ABSTRACT

Aqueous dispersed conducting polyaniline nanofiber, new electrode material for supercapacitor, is prepared employing acidic phosphate ester as dopant for nanofibrous polyaniline emeraldine base, which is synthesized by polymerization of aniline using ferric nitrate as oxidant through pseudo-high dilution technique. Highly crystalline and uniform polyaniline fibers with thin diameter of 17–26 nm are obtained, the film from which shows electrical conductivity of 32 S cm^{-1}. The thin nanofibrous polyaniline is used as electrode material for supercapacitor and its performance is evaluated in non-protonic solvent system. It shows a specific capacitance as high as 160 F g^{-1} at discharge rate of 0.4 A g^{-1} from −1 V to 1 V in 1 mol L^{-1} tetraethylammonium tetrafluoroborate/propylene carbonate solution, and the discharge/charge efficiency reaches 92%, indicating that it possesses good electrochemical reversibility. The high capacitance can be attributed to its relatively high surface area of 70 m^2 g^{-1}, which is 3–5 times higher than spherical polyaniline or thick fiberous polyaniline, leading to high utilization of the electroactive materials.

1. Introduction

Polyaniline consists of phenyl diamine and quinone diimine repeating units as shown in Scheme 1. To the best of our knowledge, polyanilines as the supercapacitors electrode materials [1] were generally doped state with selenious acid [2], graphene oxide [3] or hydrochloric acid dopant [4]. With increasing environment concern, electroactive electrode material from water soluble conducting polyaniline has attracted much attention, since the electrode preparation can be obtained in aqueous system.

Water soluble conducting polyaniline can be prepared by self-doping approach, template polymerization and counter-ion induced method [5]. Epstein and co-workers [6–8] prepared water soluble self-doped polyaniline using fuming sulfuric acid to react with emeraldine base [6] or leucoemeraldine base [7], in which the aromatic ring was covalent bonded by sulfonic acid group, giving electrical conductivity of 10^{-1}–10^{-3} S cm^{-1}. Chen et al. [8] synthesized water soluble polyaniline where the amine nitrogen in the polyaniline backbone was linked by propane sulfonic acid group, propylbenzenesulfonic acid group [9] or benzoylsulfonic group [10] by reaction of emeraldine base with 1,3-propanesultone, *p*-(3-bromopropyl)benzenesulfonic acid or *o*-sulfobenzoic anhydride, respectively. Water soluble conducting polyaniline can also be prepared using template polymerization, in which water soluble polyacrylamide [11], poly(2-acrylamido-2-methyl-1-propane-sulfonic acid) [12], poly(4-styrenesulfonate acid) [13] or poly(vinysulfonic acid) [14] was used as a binary template and hydrophilic segments. The low electrical conductivity of 10^{-8}–10^{-2} S cm^{-1}, however, was generally found since the substituents on the benzene ring or nitrogen atoms generally reduced the electrical conductivity, while the co-existence of polyaniline and insulated polymer for template polymerization was also not beneficial for high conductivity. In our previous work, we succeeded in preparing water soluble conducting polyaniline with high conductivity of 10^0–10^1 S cm^{-1} [15] through counter-ion induced method, in which acidic phosphate ester containing short hydrophilic segment was used as dopant for polyaniline emeraldine base.

Fibrilar polyanilines have been reported as electroactive electrode materials for supercapacitors due to their higher specific surface areas than those of non-fibrous polyanilines [16–19]. Among which thin polyaniline nanofibers with small diameter of 1–50 nm have attracted much attention due to their potential high capacitance, since it is natural idea that thin nanofibers can give higher specific surface area than that of thick nanofibers. Although the non-aqueous conducting polyaniline thin nanofibers doped by inorganic acid [20] or ferric sulfate [21] with a diameter of 10–23 nm have been widely investigated, only few studies were related on aqueous polyaniline nanofibers, e.g., aqueous polyaniline nanofiber colloids with a large diameter of 80–100 nm were prepared through the in situ polymerization of aniline in the presence of β-cyclodextrin by Li et al. [22].

* Corresponding author. Tel.: +86 431 85262250; fax: +86 431 85689095.
E-mail address: xhwang@ciac.jl.cn (X. Wang).

0378-7753/$ – see front matter © 2011 Elsevier B.V. All rights reserved.
doi:10.1016/j.jpowsour.2011.08.066

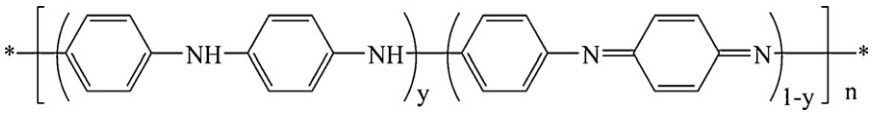

Scheme 1. Chemical structure of intrinsic polyaniline, *y* is between 0 and 1, *n* is integer.

Herein, aiming at disclosing a feasible route to prepare supercapacitor electroactive electrode materials with promising high specific capacity, aqueous conducting thin polyaniline nanofibers with small diameter of 17–26 nm were prepared, which were highly crystalline with electrical conductivity of 32 S cm^{-1}. The said thin polyaniline nanofibers serving as electrode materials for supercapacitor, gave specific capacitance as high as 160 F g^{-1} at a discharge rate of 0.4 A g^{-1}, which was much higher than those of earlier reported data from non-aqueous electrode materials, such as HCl-doped polyaniline (70 F g^{-1}) and $LiPF_6$-doped polyaniline (107 F g^{-1}) in tetraethylammonium tetrafluoroborate electrolyte solution [23].

2. Experimental

2.1. Materials

Aniline (Beijing Chemical Co.) was distilled twice under reduced pressure. Ferric nitrate was provided by Beijing Chemical Co. and used as received, other reagent was used without further treatment.

2.2. Preparation of aqueous polyaniline nanofibers

2.2.1. Preparation of polyaniline nanofibers

Polyaniline nanofibers were prepared using pseudo-high dilution approach [24], a typical process was described as follows:

1.41 g (15.0 mmol) aniline was dissolved in 15 mL of 1 mol L^{-1} nitric acid, and a 15 mL of 2.5 mol L^{-1} aqueous ferric nitrate (37.5 mmol) solution was precooled and added at a rate of 2 mL min^{-1} at 0–5 °C *via* a dropping funnel under vigorous stirring. After addition, the mixture was allowed to react for 28 h at 0–5 °C without any disturbance. The polyaniline precipitate was washed with water and ethanol several times until the filtrate was colorless. The polyaniline was added into large quantity of 1 mol L^{-1} ammonium hydroxide and stirred for 24 h, and washed with water until the filtrate was colorless. The de-doped polyaniline was dried in a vacuum at 40 °C for 48 h.

2.2.2. Preparation of aqueous conducting polyaniline nanofibers

Aqueous conducting polyaniline nanofibers dispersion was prepared according to our previous report [15]. 1.04 g (5.84 mmol) of as-prepared phosphate ester bearing one ethylene glycol unit [15a] and 0.52 g (5.77 mmol) of the above polyaniline nanofibers emeraldine base were added into 30 mL distilled water under stirring for 72 h at 60 °C. The schematic illustration of the aqueous polyaniline nanofibers was shown in Scheme 2, in which phosphate ester as anion was linked with polyaniline backbone, where the ethylene glycol hydrophilic segment assured the stability of the polyaniline dispersion.

2.3. Characterization of polyaniline nanofibers

Wide-angled X-ray diffraction (WAXD) patterns of the samples in powder were recorded using Cu Ka (λ = 1.5406 Å) radiation at 40 kV and 40 mA with D8 Advance X-ray Reflector. The data were collected in the range of 5° < 2θ < 50° with a step size of 0.1° s^{-1} and scan rate of 3° min^{-1}. UV–visible spectra (UV) were recorded on a UV-3000 spectrometer, employing polyaniline nanofibers solution in N-methyl-2-pyrrolidone or aqueous dispersion of polyaniline nanofibers. Scanning electron microscope (SEM) morphologies of the samples were carried out on an FEI XL30 ESEM field emission scanning electron microscope with operating voltage of 20 kV. Fourier transform infrared (FTIR) spectra were recorded on a Bruker TENSOR-27 spectrophotometer at a resolution of 4 cm^{-1}, a minimum of 32 scans were signal averaged, and the samples were prepared by KBr pellet. TEM image was obtained on a JEOL JEM-2010 transmission electron microscope at an acceleration voltage of 200 kV. Samples for TEM were prepared by drop casting polyaniline aqueous dispersion onto carbon-coated copper grids and allowing them to dry freely. Electrical conductivity was measured using a standard four-probe method at room temperature, in which polyaniline film from dispersion was fixed tightly on the four probes with an equal distance of 2.0 mm between adjacent probes, and the conductivity value was obtained through measuring current and voltage [25]. X-ray photoelectron spectroscopy (XPS) measurements were carried out on a VG ESCALAB MkII spectrometer with a Mg Kα X-ray source (1253.6 eV photos), where the X-ray source was operated at 14 kV and 20 mA, and the sample polyaniline film from aqueous dispersion was mounted onto standard VG sample stud with doublesided adhesive tape. The pressure in the XPS analysis chamber was maintained at 10^{-7} Pa or lower during data collection. The sample position and tilt angle were finely tuned for optimal data acquisition. The C 1s neutral carbon peak at 284.6 eV was used as the reference for all binding energies (BEs). The core-level spectrum was deconvoluted into Gaussian component peaks. The Brunauer–Emmett–Teller (BET) surface area was measured on a fully automated ASAP 2020 accelerated surface area and porosimetry analyzer (Micromeritics Co., Norcross, GA).

2.4. Preparation of working electrode and electrochemical measurements

The working electrode for supercapacitor was prepared by well mixing 9 mg as-presented aqueous dispersed polyaniline

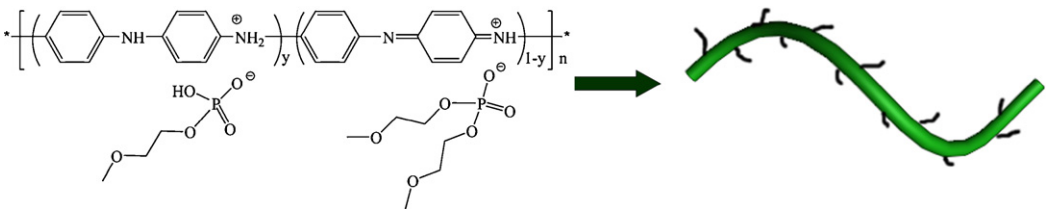

Scheme 2. Schematic illustration of aqueous dispersion of conducting polyaniline nanofibers, *y* is between 0 and 1, *n* is integer.

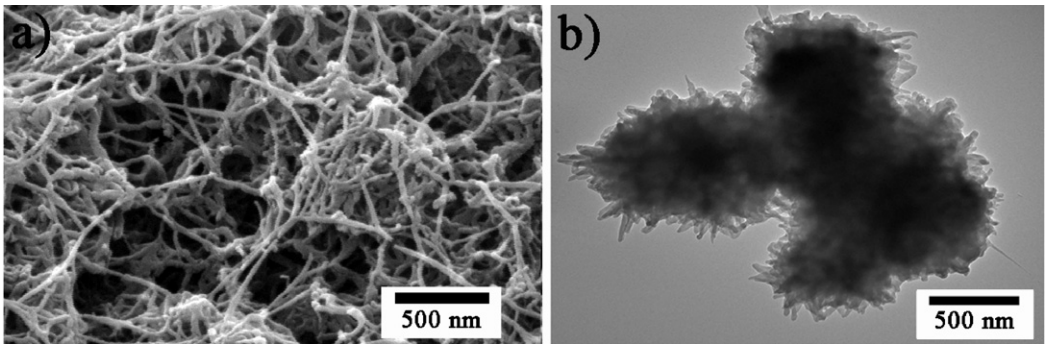

Fig. 1. SEM (a) and TEM (b) images of polyaniline nanofibers emeraldine base.

nanofibers, 1 mg cation aqueous polyurethane resin adhesion agent and 200 mg de-ionized water to make a homogeneous mixture at ambient temperature. The mixture was coated and pressed on a foam nickel to make working electrode, and then the electrode was dried at 45 °C for 72 h in vacuum oven.

All electrochemical experiments were carried out in a three-electrode glass cell with a counter electrode (platinum sheet) and a reference electrode (saturated calomel electrode). The electrolyte was 1 mol L^{-1} solution of tetraethylammonium tetrafluoroborate in propylene carbonate. Cyclic voltammetry and galvanostatic charge–discharge tests were performed on a Solartron 1287 electrochemical workstation system. Cyclic voltammogram was examined in the voltage windows ranged from −1 to 1 V versus reference electrode at a scan rate of 20 mV s^{-1}. The galvanostatic charge/discharge testing was performed from 0 to 1 V versus reference electrode at a current density of 0.4 A g^{-1}.

For comparison, aqueous dispersed polyaniline such as non-fibrous polyaniline (spherical shape) and thick polyaniline nanofibers with average diameter ranging from 25 nm to 42 nm were prepared according to our previous report [15b,24], respectively, which were used for preparation of working electrode and electrochemical testing in the same procedure as described above.

3. Results and discussion

Wan and co-workers [26] reported that the diameter of polyaniline nanofibers was strongly affected by the oxidization ability of oxidant, in which higher oxidation potential generated larger diameter.

To prepare thin polyaniline nanofibers, ferric nitrate was used as oxidant due to its lower oxidization potential of 1.28 V than that of conventional strong oxidant like ammonium persulfate [27]. Morphology of polyaniline nanofiber emeraldine base (EB) was shown in Fig. 1. Uniform nanofibers with diameters ranging from 18 to 25 nm were observed from the SEM image in Fig. 1a, and their diameters can be found through TEM image of Fig. 1b.

Unlike the separated nanofibers distribution of fibrous polyaniline
emeraldine base, fibers of aqueous conducting polyaniline were aggregated to a block, however, their fibrous shape can still be seen clearly from the circular region in Fig. 2 and their diameter ranged from 20 nm to 25 nm.

As described in Section 2, the ratio 1:1 of dopant to emeraldine base was higher than theoretical maximum doping level of 50% [28], where the extra dopant can improve the aqueous dispersion solubility [29]. The extra phosphate ester dopant distributing freely in polyaniline served as plasticizer [30] causing the aggregation of polyaniline nanofibers. To further clearly investigate the morphology of aqueous polyaniline nanofibers, the TEM of dispersion was performed and shown in Fig. 3. The uniform fibrous distribution, as well as the diameter of 21–27 nm from the circular field of Fig. 3, was consistent with that of the above SEM result.

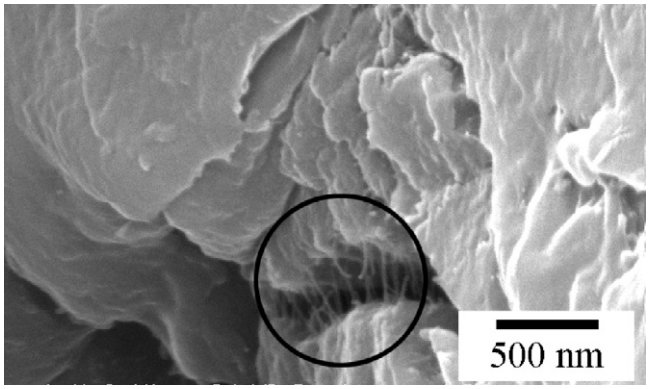

Fig. 2. Typical SEM image of polyaniline powder from as-prepared aqueous nanofibers dispersion.

The chemical structure of aqueous conducting polyaniline nanofibers is characterized by UV–visible, FTIR and XPS techniques. Fig. 4 presents the UV–visible spectra of the aqueous dispersed

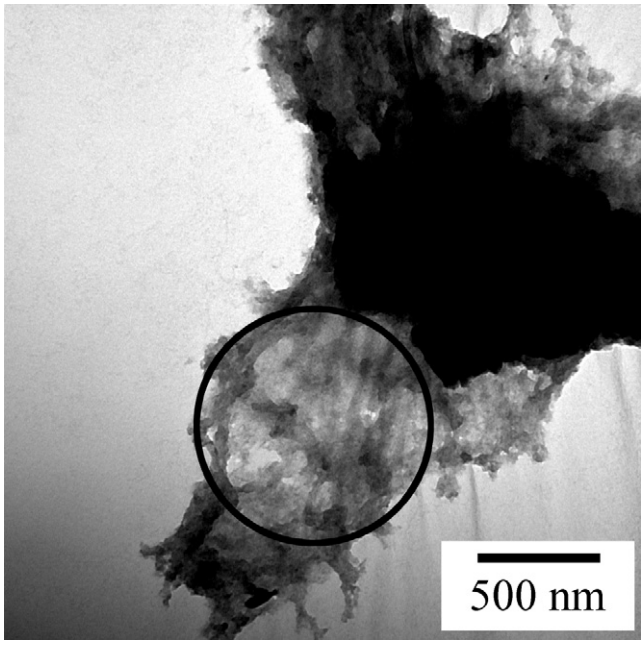

Fig. 3. Typical TEM image of as-prepared aqueous polyaniline nanofibers dispersion.

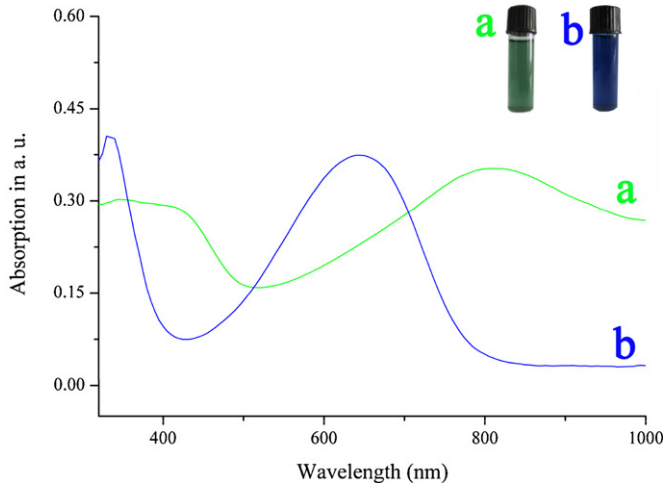

Fig. 4. UV–visible spectra of aqueous dispersion of polyaniline nanofibers (a) and polyaniline nanofiber emeraldine base in N-methyl-2-pyrrolidone solution (b).

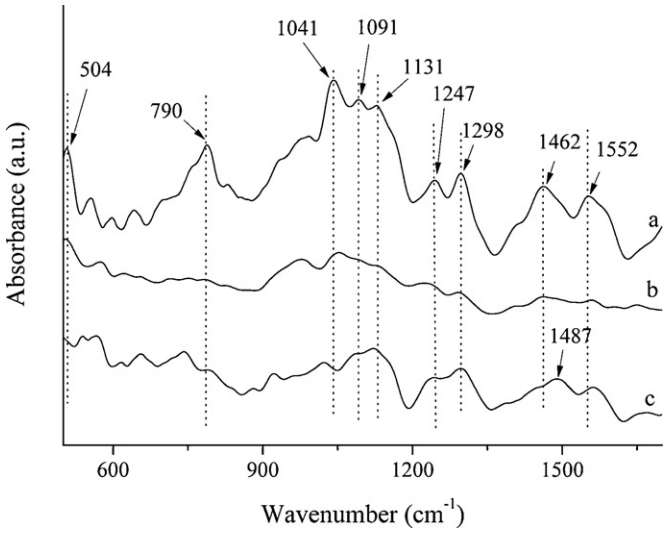

Fig. 5. FTIR spectra of polyaniline in KBr pellet: (a) as-prepared thin polyaniline nanofibers, (b) thick polyaniline nanofibers (diameter: 25 nm to 42 nm), (c) non-fibrous polyaniline.

nanofibers in water (Fig. 4a) and the fibrous polyaniline emeraldine base in N-methyl-2-pyrrolidone (Fig. 4b). Compared with the blue solution characteristic of fibrous EB form (inset b), the fibrous aqueous dispersion forms a green suspension (inset a), indicative of emeraldine salt (ES) form. Strong absorption peaks at 332 nm 646 nm were observed in EB solution (Fig. 4b), characteristic of π–π^* transition of the benzenoid structure and exciton transition of the quinoid structure [31]. As for the aqueous dispersion of polyaniline nanofibers, the absorption peak at 332 nm in EB red-shifted to broad and plateau band until to 417 nm characteristic of the semiquinoid radical cation and the peak at 646 nm in EB disappeared, instead a strong peak at 815 nm (Fig. 4a) appeared characteristics of the cationic radical polaron band [32], indicating a more extended conformation of the conducting polyaniline chains.

The FTIR spectra of various aqueous nanofibers were shown in Fig. 5, for comparison, FTIR spectra of non-fibrous spherical polyaniline and thick polyaniline nano-fibers (diameter: 25–42 nm) were shown together. The peak at 1552 cm^{-1} and 1462 cm^{-1} were consistent with C=C stretching deformation of quinoid [33] and benzene rings, respectively. These bands were similar to those found in large nanofibers and non-fibrous polyaniline, however, a red-shift of 25 cm^{-1} for benzene rings (1462 cm^{-1}) was found compared to that of 1487 cm^{-1} for non-fibrous polyaniline. The bands at 1041 cm^{-1}, 1298 cm^{-1} and 1131 cm^{-1} can be attributed to C–N stretching of secondary aromatic amine and the aromatic C–H in-plane bending. The peaks 790 cm^{-1} and 504 cm^{-1} can be assigned to the out-of-plane deformation of C–H in the 1,4-disubstituted benzene ring [34], the intensities of these peaks were stronger than that of large nanofibers and non-fibrous polyaniline. The relative intensity of 1247 cm^{-1} to 1091 cm^{-1} for P=O stretching vibration were much higher than that of large or non-fiberous polyaniline. The band at 3419 cm^{-1} can be attributed to the N–H stretching vibration in benzene ring [35]. Therefore, the results from FTIR spectra indicated that the aqueous dispersed polyaniline was in emeraldine salt form, and the phosphate ester was tightly incorporated as anions among the polyaniline backbone (see Scheme 2).

The oxidation state in polyaniline film from aqueous dispersed nanofibers was investigated by XPS technique, the XPS spectra as well as the model fits were shown in Fig. 6. From the curve of binding energy from 1 eV to 1200 eV in Fig. 6a, the polyaniline nanofibers were composed of C, N, O, Fe and P elements. The strong peak at 133.5 eV can be assigned as P 2p (inset in Fig. 6a), in which its full width at half maximum (FWHM) was 1.8 eV, and the integral area was 6951.8, indicating that the phosphate ester was linked with the polyaniline backbone, which provided a strong support for the polyaniline structure as shown in Scheme 2, consistent with the result of FTIR and UV–visible spectra. As shown in Fig. 6b, the asymmetric N 1s core level can be deconvoluted into four peaks, locating

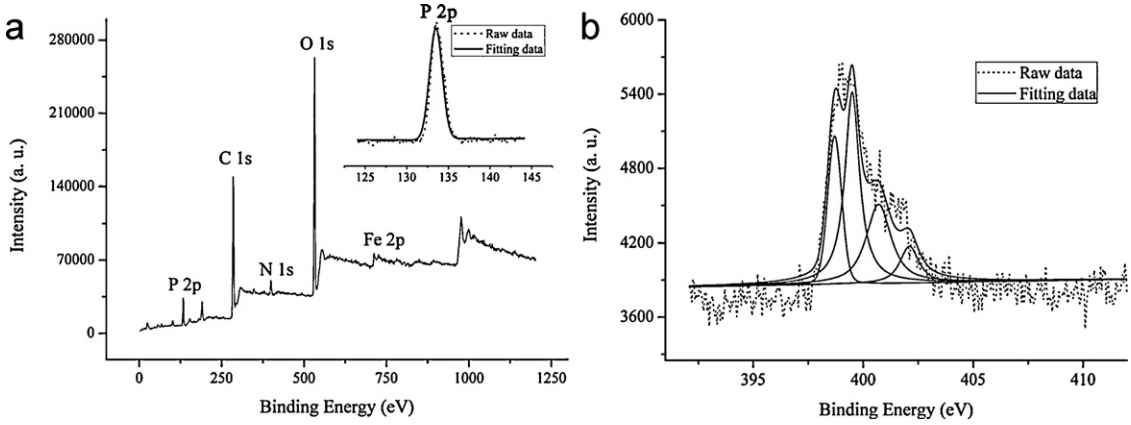

Fig. 6. XPS patterns of polyaniline nanofibers film from aqueous dispersion. (a) Wide binding energy, (b) N 1s core-level spectra.

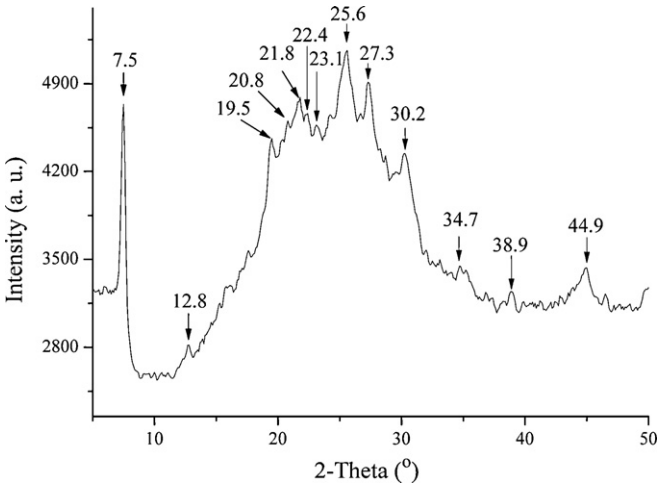

Fig. 7. The WAXD pattern of polyaniline nanofibers powder from dispersion.

at 398.7 eV, 399.5 eV, 400.7 eV and 402.1 eV, assigned to quinoid imine (=N=), benzenoid amine (–NH–), the protonated nitrogen atoms with iminium ions (–NH^+=) and ammonium ion (–NH_2^+–) [28], respectively. The integral area of the four peaks was 1015.3, 1938.0, 1268.7 and 445.0, respectively. The area fraction of these four peaks was 0.22, 0.41, 0.27 and 0.10, respectively, where the total area from protonated nitrogen atoms was 37%, indicating that the doping level of polyaniline was 37%. It should be noted that the integral area of P 2p was nearly one time higher than the total area of the four peaks, while the 37% doping level indicated that only 37% phosphate ester dopant served as anion to link with the polyaniline backbone, therefore, much more excess phosphate ester was freely distributed in polyaniline domain.

The crystalline structure of aqueous polyaniline nanofibers was studied by WAXD. As shown in Fig. 7, the sharp peaks centered at $2\theta = 19.5^\circ$ and $2\theta = 25.6^\circ$ were assigned as the periodicity parallel to the polyaniline chains [36] and the periodicity perpendicular to the polyaniline chain [37], respectively, indicating that the polyaniline nanofibers were highly crystalline. The peaks such as $2\theta = 20.8^\circ$, 21.8°, 22.4°, 23.1°, 27.3°, 30.2°, 34.7°, 38.9° and 44.9° might be caused by the branches of dopant interacting with polyaniline chain at various directions [38]. The peaks at $2\theta = 7.5^\circ$ and 12.8° were observed, the relatively high intensity of peak at 7.5° was due to a bilayer of phosphate ester side chains with a limited interdigitation, and the sharp peak at 12.8° was assigned as the periodic distance between the dopant and the N atom on adjacent main chain. This ordered lamellar structure composed of alternating layers of rigid polyaniline chain and flexible phosphate ester side chains was also observed in aqueous non-fibrous conducting polyaniline [15a]. A high electrical conductivity of polyaniline films of 32 S cm^{-1} was obtained due to their crystalline structure, which was 1–2 order of magnitude higher than that of the 0.1–5 S cm^{-1} from the typical dopant state with Li dopant [39] and one order of magnitude higher than that of 4.5 S cm^{-1} from water soluble spherical polyaniline [15b].

To estimate the electrochemical performance of working electrode made of various polyanilines (thin polyaniline nanofibers, thick polyaniline nanofibers, and non-fibrous polyanilines), corresponding cyclic voltammetric curves and galvanostatic charge/discharge curves were recorded and shown in Fig. 8. The cyclic voltammetric curves were obtained from −1 V to 1 V versus saturated calomel reference electrode at scan rate of 20 mV s^{-1} and shown in Fig. 8A. The thin polyaniline nanofibers showed considerably higher redox currents than those of thick polyaniline nanofibers or non-fibrous spherical polyaniline, indicating that more effective surface areas of the thin polyaniline nanofibers were accessible for the electrolytes [40].

Galvanostatic charge/discharge at density of 0.4 A g^{-1} was performed on the device in order to further understand the possibility of the obtained polyaniline nanofibers for supercapacitors applications. Typical galvanostatic charge/discharge curves of polyaniline nanofibers electrode were presented in Fig. 8B. The discharge capacitance (C_m) can be calculated according to Eq. (1) [41],

$$C_m = \frac{C}{m} = \frac{(I \times \Delta t)}{(\Delta V \times m)} \quad (1)$$

where C_m was specific capacitance, I was charge/discharge current, Δt was the discharge time, ΔV was 1 V, and m was the mass of electroactive electrode materials.

A capacitance of 160 F g^{-1} was obtained for the thin nanofibrous polyaniline, which was higher than that of 120 F g^{-1} for thick nanofibrous polyaniline or that of 90 F g^{-1} for spherical (non-fibrous) polyaniline. A large Brunauer–Emmett–Teller surface area of 70 m^2 g^{-1} for the thin polyaniline nanofibers was obtained, which was much higher than that of 21 m^2 g^{-1} for thick nanofibers or 13 m^2 g^{-1} for spherical polyaniline. The higher specific capacitances can be attributed to their higher specific surface areas of the thin polyaniline nanofibers, which led to the higher utilization of the active materials.

On the other hand, discharge/charge efficiency γ can be calculated according to the following formula:

$$\gamma(\%) = \frac{\Delta t}{\Delta t'} \quad (2)$$

where Δt was the discharge time, $\Delta t'$ was the charge time.

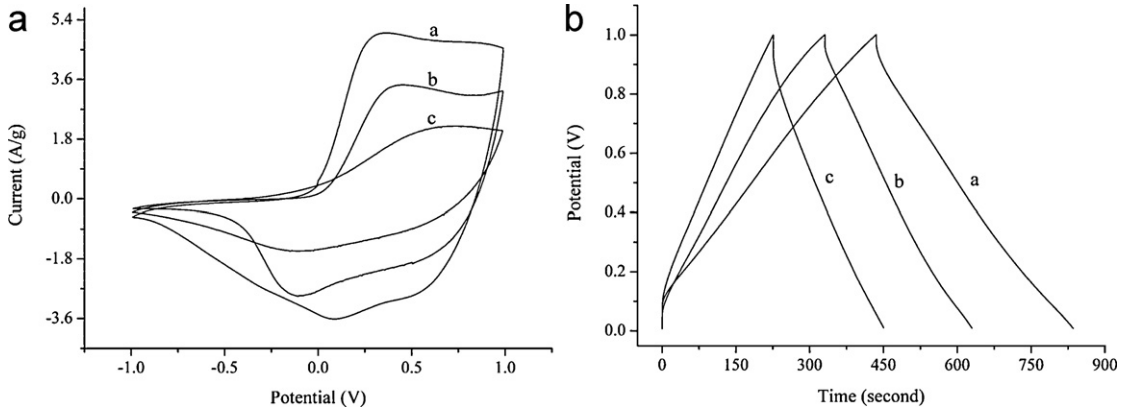

Fig. 8. (A) Cyclic voltammograms and (B) galvanostatic charge/discharge curves for (a) as-prepared thin polyaniline nanofiber electrode, (b) thick polyaniline nanofiber electrode and (c) non-fibrous polyaniline electrode. Scan rate for cyclic voltammograms: 20 mV s^{-1}. Current density for galvanostatic charge/discharge: 0.4 A g^{-1}.

The thin polyaniline nanofibers electrode exhibited high discharge/charge efficiency of 92%, indicating good electrochemical reversibility and discharge/charge rate control capability.

4. Conclusion

In summary, aqueous conducting polyaniline nanofibers were prepared using acidic phosphate ester containing hydrophilic ethylene glycol segment to dope nanofibrous de-doped polyaniline, in which the fibers was synthesized by the ferric nitrate as oxidant through pseudo-high dilution method. The conducting polyaniline nanofibers showed a uniform thin diameter of 17–26 nm with high electrical conductivity of $32\,S\,cm^{-1}$. Supercapacitors electrode made from thin nanofibrous polyaniline gave a high specific capacitance of $160\,F\,g^{-1}$ at a discharge rate of $0.4\,A\,g^{-1}$ within the potential range of −1 to 1 V versus saturated calomel reference electrode in organic non-protonic electrolyte solution, which was higher than that of thick nanofibrous or spherical polyaniline. The high specific capacitance can be ascribed to its higher utilization of the active materials, since a large BET surface area of $70\,m^2\,g^{-1}$ was obtained for the thin nanofibrous polyaniline, which was higher than that of thick nanofibers or spherical polyaniline. The electrode material also showed high discharge/charge efficiency of 92%, indicating that thin nanofibrous polyaniline possessed good electrochemical reversibility and discharge/charge rate-control capability.

Acknowledgment

We thank the National Science Foundation of China for financial support through Project No. 51073156 and 51021003.

References

[1] G.A. Snook, P. Kao, A.S. Best, J. Power Sources 196 (2011) 1.
[2] C.A. Amarnath, J.H. Chang, D. Kim, R.S. Mane, S.H. Han, D. Sohn, Mater. Chem. Phys. 113 (2009) 14.
[3] H.L. Wang, Q.L. Hao, X.J. Yang, L.D. Lu, X. Wang, Electrochem. Commun. 11 (2009) 1158.
[4] X. Zhang, W.J. Goux, S.K. Manohar, J. Am. Chem. Soc. 126 (2004) 4502.
[5] (a) Y. Cao, P. Smith, A.J. Heeger, Synth. Met. 48 (1992) 91;
(b) A.J. Heeger, Synth. Met. 55–57 (1993) 3471.
[6] (a) J. Yue, Z.H. Wang, K.R. Cromack, A.J. Epstein, A.G. MacDiarmid, J. Am. Chem. Soc. 113 (1991) 2665;
(b) J. Yue, A.J. Epstein, J. Am. Chem. Soc. 112 (1990) 2800;
(c) P.K. Kahol, A. Raghunathan, B.J. McCormick, A.J. Epstein, Synth. Met. 101 (1999) 815;
(d) W. Lee, G. Du, S.M. Long, S. Shimizu, T. Saitoh, M. Uzawa, A.J. Epstein, Synth. Met. 84 (1997) 807;
(e) J. Yue, A.J. Epstein, A.G. Macdiarmid, Mol. Cryst. Liq. Cryst. 189 (1990) 255.
[7] (a) X.L. Wei, A.J. Epstein, Synth. Met. 74 (1995) 123;
(b) X.L. Wei, Y.Z. Wang, S.M. Long, C. Bobeczko, A.J. Epstein, J. Am. Chem. Soc. 118 (1996) 2545;
(c) X.L. Wei, M. Fahlman, A.J. Epstein, Macromolecules 32 (1999) 3114.
[8] (a) S.A. Chen, G.W. Hwang, J. Am. Chem. Soc. 117 (1995) 10055;
(b) S.A. Chen, G.W. Hwang, J. Am. Chem. Soc. 116 (1994) 7939.
[9] M.Y. Hua, Y.N. Su, S.A. Chen, Polymer 41 (2000) 813.
[10] H.K. Lin, S.A. Chen, Macromolecules 33 (2000) 8117.
[11] P. Ghosh, A. Chakrabarti, S.K. Siddhanta, Eur. Polym. J. 35 (1999) 803.
[12] (a) L. Sun, H. Liu, R. Clark, S.C. Yang, Synth. Met. 84 (1997) 67;
(b) K.S. Lee, G.B. Blanchet, F. Gao, Y.L. Loo, Appl. Phys. Lett. 86 (2005) 074102.
[13] Y. Li, B.Y. Ying, L.J. Hong, M.J. Yang, Synth. Met. 160 (2010) 455.
[14] Y.P. Shen, J.Z. Sun, J.G. Wu, Q.Y. Zhou, J. Appl. Polym. Sci. 96 (2005) 814.
[15] (a) H.M. Zhang, X.H. Wang, J. Li, Z.S. Mo, F.S. Wang, Polymer 50 (2009) 2674;
(b) J. Luo, H.M. Zhang, X.H. Wang, J. Li, F.S. Wang, Macromolecules 40 (2007) 8132;
(c) H.M. Zhang, J.L. Lu, X.H. Wang, J. Li, F.S. Wang, Polymer 52 (2011) 3059.
[16] (a) S. Liu, X.H. Liu, Z.P. Li, S.R. Yang, J.Q. Wang, New J. Chem. 35 (2011) 369;
(b) P.J. Hung, K.H.Y. Chang, F. Lee, C.C. Hu, K.M. Lin, Electrochim. Acta 55 (2010) 6015.
[17] H. Guan, L.Z. Fan, H.C. Zhang, X.H. Qu, Electrochim. Acta 56 (2010) 964.
[18] Q. Wu, Y.X. Xu, Z.Y. Yao, A.R. Liu, G.Q. Shi, ACS Nano 4 (2010) 1963.
[19] H.Y. Mi, X.G. Zhang, S.D. Yang, X.G. Ye, J.M. Luo, Mater. Chem. Phys. 112 (2008) 127.
[20] Z.M. Zhang, J.Y. Deng, M.X. Wan, Mater. Chem. Phys. 115 (2009) 275.
[21] H.J. Ding, Y.Z. Long, J.Y. Shen, M.X. Wan, J. Phys. Chem. B114 (2010) 115.
[22] X.W. Li, T. Zhuang, G.C. Wang, Y.P. Zhao, Mater. Lett. 62 (2008) 1431.
[23] K.S. Ryu, K.M. Kim, N.G. Park, Y.J. Park, S.H. Chang, J. Power Sources 103 (2002) 305.
[24] H.M. Zhang, X.H. Wang, J. Li, F.S. Wang, Synth. Met. 159 (2009) 1508.
[25] P.D. Gaikwad, D.J. Shirale, V.K. Gade, P.A. Savale, H.J. Kharat, K.P. Kakde, S.S. Hussaini, N.R. Dhumane, M.D. Shirsat, Bull. Mater. Sci. 29 (2006) 169.
[26] H.J. Ding, M.X. Wan, Y. Wei, Adv. Mater. 19 (2007) 465.
[27] H.J. Ding, Y.Z. Long, J.Y. Shen, M.X. Wan, J. Phys. Chem. B 114 (2010) 115.
[28] J. Yuet, A.J. Epstein, Macromolecules 24 (1991) 4441.
[29] B.Z. Hsieh, H.Y. Chuang, L. Chao, Y.J. Li, Y.J. Huang, P.H. Tseng, T.H. Hsieh, K.S. Ho, Polymer 49 (2008) 4218.
[30] J. Laska, K. Zak, A. Pron, Synth. Met. 84 (1997) 117.
[31] P. Wang, K.L. Tan, E.T. Kang, K.G. Neoh, Appl. Surf. Sci. 193 (2002) 36.
[32] S.A. Chen, H.T. Lee, Macromolecules 28 (1995) 2858.
[33] Y.J. He, Mater. Chem. Phys. 92 (2005) 134.
[34] (a) Z.A. Hu, Y.L. Xie, Y.X. Wang, L.P. Mo, Y.Y. Yang, Z.Y. Zhang, Mater. Chem. Phys. 114 (2009) 990;
(b) Y.Z. Li, X. Zhao, Q. Xu, Q.H. Zhang, D.J. Chen, Langmuir 27 (2011) 6458.
[35] S.G. Kim, J.W. Kim, H.J. Choi, M.S. Suh, M.J. Shin, M.S. Jhon, Colloid Polym. Sci. 278 (2000) 894.
[36] J.P. Pouget, M.E. Jozefowicz, A.J. Epstein, X. Tang, A.G. MacDiarmid, Macromolecules 24 (1991) 779.
[37] Y.B. Moon, Y. Cao, P. Smith, A.J. Heeger, Polym. Commun. 30 (1989) 196.
[38] D.X. Han, Y. Chu, L.K. Yang, Y. Liu, Z.X. Lu, Colloids Surf. A: Physicochem. Eng. Aspects 259 (2005) 179.
[39] (a) J. Stejskal, R.G. Gilbert, Pure Appl. Chem. 74 (2002) 740;
(b) K.S. Ryu, K.M. Kim, Y.J. Park, N.G. Park, M.G. Kang, S.H. Chang, Solid State Ionics 152 (2002) 861.
[40] J.L. Liu, M.Q. Zhou, L.Z. Fan, P. Li, X.H. Qu, Electrochim. Acta 55 (2010) 5819.
[41] Y.G. Wang, Y.Y. Xia, J. Electrochem. Soc. 153 (2006) A450.